

Size and orientation dependence in the electronic properties of silicon nanowires

Jia-An Yan, Li Yang,* and M. Y. Chou

School of Physics, Georgia Institute of Technology, Atlanta, Georgia 30332-0430, USA

(Received 10 December 2006; revised manuscript received 28 May 2007; published 17 September 2007)

By using first-principles pseudopotential methods, we have studied the electronic properties of hydrogen-passivated silicon nanowires along the [100], [110], and [111] directions with diameter up to 3.4 nm. It is found that as the diameter decreases, the energy band gaps are distinctly enlarged due to the confinement effect. The valence-band maximum moves down while the conduction-band minimum moves up compared with the bulk. By using the many-body perturbation theory within the *GW* approximation, we have also investigated the self-energy correction to the energy band gaps. Our calculational results show that, although the band gap values strongly depend on both the diameter and orientation, the *GW* corrections are mainly dependent on diameter and less sensitive to the growth orientation. The effective mass as a function of diameter is also discussed.

DOI: [10.1103/PhysRevB.76.115319](https://doi.org/10.1103/PhysRevB.76.115319)

PACS number(s): 73.21.Hb, 73.22.Dj, 78.67.Lt

I. INTRODUCTION

Silicon nanowires (SiNWs) are one of the promising building blocks for future nanoelectronic and nanophotonic devices, and have attracted extensive attention in recent years due to their compatibility with Si-based electronic technology.^{1–6} Nanoscale devices based on individual homogeneous nanowires have been demonstrated in experiment, such as field-effect transistors,² logic circuits,⁷ sensors,⁸ lasers,⁹ and light-emitting diodes.¹⁰ As the diameter of synthesized SiNWs shrinks to a few nanometers,^{3,4,11,12} the quantum size effect becomes important. Photoluminescence data revealed a substantial blueshift in nanowires with decreasing size.^{13,14} Recent scanning-tunneling spectroscopy data^{3,4} also showed a significant increase in the electronic energy gap for very thin semiconductor nanowires, explicitly demonstrating the quantum size effect. Recent experiments have shown that SiNWs can be grown along the [100], [110], [111], and [112] directions.^{2,4,10}

Due to the strong quantum confinement effect in ultrathin SiNWs, the electronic properties in this system may show different features as opposed to a bulk material, and consequently affect the nanoelectronic device characteristics. In fact, recent calculations have already shown that the parabolic effective-mass model with bulk effective masses significantly overestimates the threshold voltages of ballistic silicon nanowire transistors (SNWTs) when the wire width is less than 3 nm.^{15,16} Therefore, it is strongly desirable to study the quantum size effects on the electronic properties (e.g., effective mass, band gaps, and band edges) in order to better understand the mobility of carriers and to facilitate the design of nanoelectronic devices.

Previous density-functional calculations have been performed to study the electronic structure of [001] and [111] oriented SiNWs with diameters less than 1.5 nm,^{17–20} in an effort to understand the photoluminescence of porous silicon in the visible range. However, the diameters of the wires considered in these first-principles studies were too small to study the transitional trend to the bulk. More recently, Vo *et al.*²¹ performed first-principles simulations for the [100], [110], and [111] SiNWs, focusing mainly on the effect of

surface reconstructions on the structural and electronic properties of the nanowires. By density-functional calculations of [100] SiNWs, Ruruli *et al.*²² found that the specific surface reconstruction can even lead to the surface states crossing the Fermi level and consequently make the wire metallic and/or semimetallic. The electronic structures and optical properties near the gaps for SiNWs with the [001] and [111] orientations are also reported.²³ In addition, Cao *et al.*²⁴ investigated the stable geometries for pristine Si nanowires grown along the [100] axis and found that Si nanowires with diameters smaller than 1.7 nm prefer a shape with square cross section.

In this paper, we present a comprehensive study on the hydrogen-passivated SiNWs oriented along the [100], [110], and [111] directions using the density-functional theory (DFT) with the local-density approximation (LDA) and the many-body perturbation method based on the *GW* approximation. Some related results have been published in Ref. 25. In this work, we focus on the modification of the electronic properties. We will address in detail the following two questions: (i) how the electronic properties depend on the size of the nanowire, and (ii) how the electronic properties change with respect to the different orientations of the nanowires. The organization of the paper is as follows: we first give the calculational details in Sec. II. We then discuss our results in Sec. III and conclude in Sec. IV.

II. CALCULATIONAL DETAILS

A. Local-density approximation calculations

Silicon nanowires with various cross-sectional shapes and axial orientations have been synthesized by different experimental groups.^{4,26,27} These SiNWs usually have an approximately cylindrical shape with chemical passivation on the surface. We construct our cylindrical wire models from the bulk and passivate all Si dangling bonds on the surface by H atoms in such a way that no complex of SiH₃ is present. Relaxations are performed to reduce the forces to within 0.02 eV/Å, and the lattice constant along the *z* direction is optimized by minimizing the stress. Summarized in Table I are the diameters (after relaxation) of the wires and the num-

TABLE I. Diameter d (in nm) and the number of Si and H atoms for the wires in our calculations. The diameter d is defined as twice the average distance of the terminating hydrogen atom to the wire center.

100				110				111			
No.	d	Si	H	No.	d	Si	H	No.	d	Si	H
1	0.91	16	18	1	1.08	16	12	1	1.16	38	30
2	1.05	21	20	2	1.74	42	20	2	1.60	74	42
3	1.29	30	26	3	2.31	76	28	3	2.04	122	54
4	1.40	37	28	4	2.81	110	36	4	2.60	218	78
5	1.87	69	36	5	3.46	172	44	5	3.02	302	90
6	2.26	97	44					6	3.40	398	102
7	2.60	137	52								
8	3.34	221	68								

ber of atoms in the supercells used in our calculations. The diameter d is defined as twice the average distance of the terminating hydrogen atom to the wire center. For the two [100] SiNWs with $d=0.91$ nm and $d=1.29$ nm, the cross sections are not exactly cylindrical, which will strongly affect the effective masses of electrons and holes.

Our LDA calculations within DFT are carried out using norm-conserving pseudopotentials²⁸ with a plane-wave basis. Periodic-boundary conditions are employed in the xy plane with a supercell large enough (the wire separation is more than 6 Å in LDA calculations and more than 12 Å in GW calculations) to eliminate the interaction between neighboring wires. The energy cutoff for the plane waves is 12 Ry. This energy cutoff has been tested to converge the energy gap to within 0.05 eV in LDA calculations. The convergence of the GW energy gap is found to be within 0.04 eV. The Monkhorst-Pack k -point mesh of $1 \times 1 \times 8$ is found to provide sufficient accuracy for the calculated total energies and forces. For the following GW calculations, the $1 \times 1 \times 16$ k -point sampling gives a converged energy gap. After the atomic configurations of SiNWs are fully relaxed, the electronic structure of SiNWs is calculated. The LDA wave functions and eigenvalues are employed as a starting point for the following GW calculations.

B. GW calculations

The Kohn-Sham energy gap can be corrected by evaluating the self-energy operator in the GW approximation.²⁹ In this calculation, dynamic dipole-dipole interactions between the supercells can occur even for systems without permanent dipoles. This interaction is long ranged and attenuates very slowly with respect to the supercell size. Therefore, the convergence of GW calculations for atoms and clusters with respect to the supercell size can be very slow (see, e.g., the discussion by Onida *et al.* in Ref. 30).

In this study, we truncate the Coulomb interaction between neighboring nanowires in a cylindrical geometry.^{31,32} Specifically, the Coulomb interaction $v(\mathbf{r})=e^2/|\mathbf{r}|$ in real space is truncated as

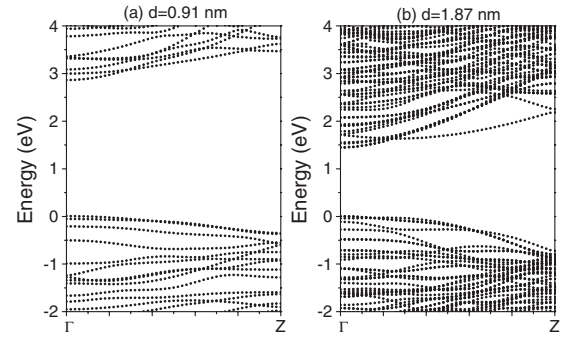


FIG. 1. Energy band structure in LDA for SiNWs along [100] with diameters of (a) 0.91 nm and (b) 1.87 nm. The valence-band maximum has been shifted to zero.

$$v_c(\mathbf{r}) = \frac{e^2}{|\mathbf{r}|} \theta(\rho - \rho_c) \theta(|z| - z_c), \quad (1)$$

where $\rho = \sqrt{x^2 + y^2}$ is the radial coordinate perpendicular to the wire axis (\hat{z}). This kind of Coulomb truncation techniques has been successfully employed to study, e.g., the GW corrections as well as the excitonic effects in carbon nanotube.³² In our calculations, the truncation cutoff ρ_c equals to half the center-to-center interwire distance R , ensuring that $d_{\max} < \rho_c < R - d_{\max}$, with d_{\max} the maximum diameter of the nanowire. This requires that the supercell on the xy plane be at least twice as large as the wire itself: $R > 2d_{\max}$. As for the cutoff z_c , it has to be smaller than the effective supercell size along the wire direction, which is dictated by the number of discretized k points used to sample the Brillouin zone along \hat{z} . We found that the GW corrections in Si nanowires are not sensitive to this parameter, whereas its importance in studying the excitonic effects has been demonstrated.³²

We have calculated the GW quasiparticle gaps (E_g^{GW}) for a few thin SiNWs: $d=1.08$ and 1.74 nm silicon nanowires in the [110] direction; $d=1.16$ nm in the [111] direction; and $d=0.91$, 1.05, and 1.29 nm in the [100] direction. A GW calculation is also performed for bulk silicon as a reference.

III. RESULTS AND DISCUSSIONS

A. Band structure and band gaps

In Figs. 1–3, we show typical energy bands for the [100], [110], and [111] nanowires, respectively. One evident feature is that for the thin SiNWs, all the band gaps are direct. Bulk Si is known to have an indirect band gap of 1.17 eV, with the conduction-band minima located at about 85% along Γ to X . Therefore, there are six equivalent conduction-band minima on $\pm x$, $\pm y$, and $\pm z$ axes, with a transverse mass (0.1905 of the free-electron mass m_e) much less than the longitudinal mass (0.9163 m_e).

For the [100] wires, four minima on $\pm y$ and $\pm z$ will be projected onto $\bar{\Gamma}$ due to band folding and thus yields a direct band gap, as shown in Fig. 1. When [110] wires are formed, two of these minima on $\pm z$ will be projected onto the $\bar{\Gamma}$ point of the one-dimensional Brillouin zone. Based on the

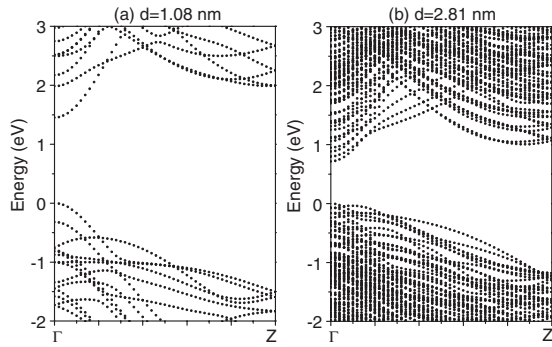


FIG. 2. Energy band structure in LDA for SiNWs along [110] with diameter of (a) $d=1.08$ nm and (b) $d=2.81$ nm. The valence-band maximum has been shifted to zero.

effective-mass approximation, both the large and the small masses appear in the confinement plane, with the larger longitudinal mass being the relevant effective mass for describing the confinement effect in the cross-section plane. On the other hand, the four remaining minima will be projected to a point between Γ and the zone boundary (Z), with the effective mass on the confinement plane being a value between the longitudinal and transverse masses. Therefore, the conduction-band edge at Γ is expected to have a smaller upward shift induced by confinement and the band gap becomes direct.

In contrast, the projection along the [111] direction is expected to produce an indirect gap in large [111] wires. The [111] nanowire shows an indirect to direct transition as the diameter of SiNWs decreases. The transition occurs at about $d=2.2$ nm, as can be seen in Fig. 4. However, the difference between the indirect and direct gaps is very small (less than 0.05 eV), making the determination of the exact transition point difficult.

Figure 5 summarizes the LDA (direct) band gap versus diameter of SiNWs, showing the size dependence of the band gap for the [100], [110], and [111] wires. Apparently, the energy gap is significantly increased for thin nanowires by quantum confinement. In addition to the size dependence, the energy gap also shows different change with respect to the growth orientation. The band gaps of [100] and [111]

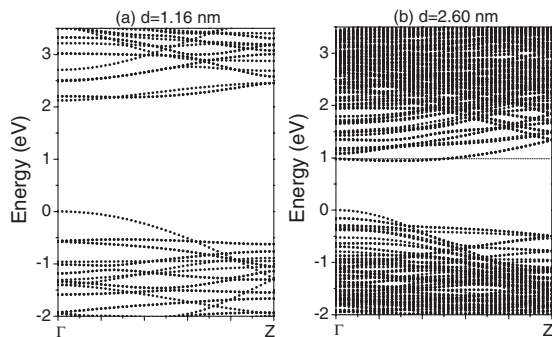


FIG. 3. Energy band structure in LDA for SiNWs along [111] with diameters of (a) 1.16 nm and (b) 2.60 nm. The valence-band maximum has been shifted to zero. Horizontal dotted line indicates conduction edge at Γ .

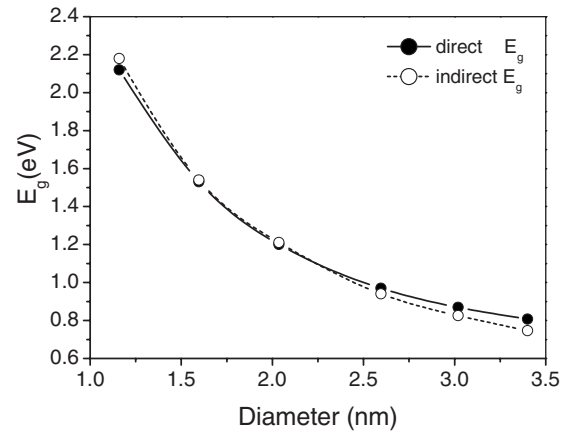


FIG. 4. Direct and indirect energy gaps versus diameter for the [111] SiNWs.

nanowires are rather close, while distinctly larger than that for the [110] wires.

In Fig. 5, we also show the GW corrections to the energy band gaps for several thin SiNWs. For bulk silicon, $E_g^{\text{LDA}}=0.58$ eV, as indicated by the solid line in Fig. 5. The GW correction is about 0.5 eV, which uplifts the gap to 1.08 eV. Both the LDA gaps and the GW corrections greatly increase as d decreases, clearly showing the effect of quantum confinement. The dependence on the diameter d can be described by

$$E_g = E_{g,\text{bulk}} + C(1/d)^\alpha, \quad (2)$$

as proposed by Delerue *et al.*,³³ where $E_{g,\text{bulk}}$ is the bulk gap value from LDA or GW. The exponent α is expected to be equal to 2 using an effective-mass particle-in-a-box approach when the barrier height is infinite.³⁴ The fitted results are smaller than 2, as listed in Table III. The fitting data set has included the bulk value as the limit, i.e., $E_g^{\text{g,bulk}}=0.58$ (LDA) and 1.08 eV (GW) for $d=\infty$ (in real fitting, $d=8$ nm are

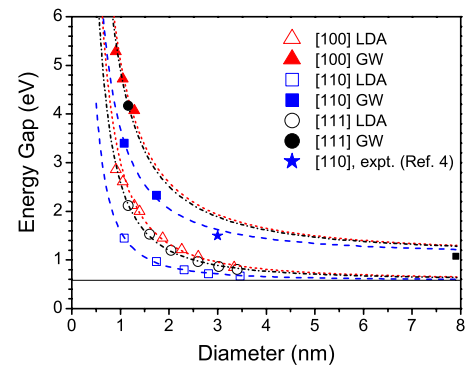


FIG. 5. (Color online) Energy band gap versus diameter for the [100] (Δ), [110] (\square), and [111] (\circ) SiNWs, compared with the measured gap for a [110] wire (\star). The dashed, dash-dotted, and short dashed lines are fitted to the data points (see text). The fitted results are listed in Table III. The LDA band gap of bulk Si is indicated by the solid line, and the bulk GW gap is marked around $d=8.0$ nm.

TABLE II. *GW* corrections (in eV) to the LDA band gaps for the [100], [110], and [111] nanowires.

	d (nm)	E_g^{LDA}	E_g^{GW}	<i>GW</i> corrections
[100]	0.91	2.86	5.28	2.42
	1.05	2.61	4.72	2.11
	1.29	2.21	4.07	1.86
[110]	1.08	1.45	3.40	1.95
	1.74	0.97	2.33	1.36
[111]	1.16	2.12	4.17	2.05

used). From Table III, we can see that for LDA α is found to be approximately 1.7, while for the *GW* α is 1.4, smaller than the LDA result. Clearly, the dependence of *GW* corrections on the size of nanowires is different as compared with LDA results.

The calculated *GW* corrections are listed in Table II. It can be seen that these are much larger than the correction found in the bulk. With increasing diameter, the band gaps decrease to the bulk *GW* value of 1.08 eV. The self-energy correction, which increases monotonically with decreasing diameter, exhibits a rather strong size dependence. In the past, this important variation has been neglected by postulating a size independent constant correction that is usually obtained from the bulk.²⁰ This approximation will inevitably introduce significant errors in the calculated optical gaps.

Bruno *et al.*³⁶ recently reported the calculated *GW* band gaps for a few small Si nanowires. The results are systematically smaller than those presented in this paper by 0.5 eV or more. The origin of this discrepancy is not clear since different computational codes were used. We note that, as demonstrated by Rozzi *et al.*,³⁷ if the Coulomb interaction is not fully truncated in a supercell setting, one may obtain a gap for a nanowire that is too small compared with the converged value.

The reason for the size dependence of *GW* corrections can be understood as follows. Within the *GW* approximation, the self-energy Σ is determined as $\Sigma = iGW$, with G being the single-particle Green's function and W the screened Coulomb interaction calculated using the dielectric screening matrix ϵ within the random-phase approximation. The real part of Σ splits into two contributions: $\text{Re}\Sigma = \Sigma_{\text{SEX}} + \Sigma_{\text{COH}}$, where the screened exchange (SEX) part arises from the

TABLE III. Obtained fitting parameters in Eq. (2) for the energy gap as a function of diameter.

Parameter	[100]		[110]		[111]	
	LDA ^a	GW ^b	LDA	GW	LDA	GW ^c
C	2.4	4.0	1.0	2.6	2.0	3.8
α	1.7	1.4	1.8	1.4	1.7	1.4

^aExcluding the first two data points.

^bExcluding the first data point.

^cThe exponential fixed at the same value as the [100] wires.

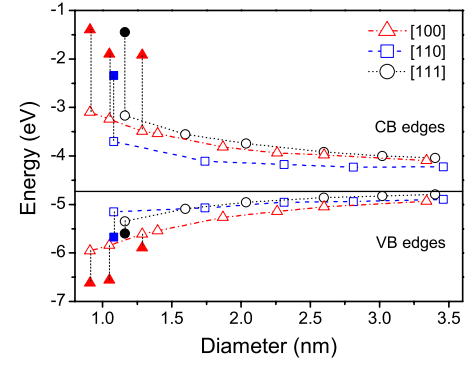


FIG. 6. (Color online) Valence- and conduction-band edges (calculated by LDA) versus diameter for SiNWs. The solid symbols show the *GW*-corrected values. The bulk limit for the valence-band edge estimated by the average work function is also shown by the horizontal solid line.

poles in the Green's function and the Coulomb-hole (COH) part from the poles in the screened interaction. Detailed analyses show that the screened exchange term dominates the self-energy corrections, indicating that the origin of the size dependency for the *GW* corrections mainly comes from the highly confined wave function.

In addition to the size dependence, both the LDA and *GW* energy band gaps exhibit strong orientation dependence. For the same diameter, the [100] wire has the largest E_g , while [110] wire the lowest. Both LDA and *GW* results show that the [111] wire has the band gap close to the [100] wire. The [111] and [100] curves are nearly overlapped.

In contrast, the *GW* corrections are not sensitive to the growth orientation. This important feature can be clearly seen from Fig. 5, where the [100] and [111] curves are almost overlapped in both LDA and *GW* contexts. For different growth orientations, the *GW* corrections are very close for a given size, as shown in Table II. The reason for this similarity is from the highly confined electronic wave functions. The confinement enhances the screened exchange term and dominates the *GW* correction values. As a result, the correction of quasiparticle band gap is not sensitive to the direction but to the size of wire.

The energy levels of valence-band (VB) maximum and conduction-band (CB) minimum at Γ are expressed relative to the vacuum level ϕ . The vacuum level ϕ is determined from the average local potential in the vacuum region where it approaches a constant in the supercell. Figure 6 shows the change of CB and VB edges with respect to the wire diameter. As the diameter decreases, the valence-band edge moves down, while the conduction-band minimum moves up. Consequently, the wire band gap is enlarged for the thinner nanowires. However, the band edge variations are somewhat different for different growth orientations. With decreasing diameter, both the conduction and valence-band edges of the [100] and [111] wires show clear modifications, indicating that the band edges are sensitive to size. In contrast, in the [110] wires the valence-band edges are almost flat, while the conduction-band edges increase more significantly with decreasing diameter. The bulk limit for the valence-band edge can be estimated by the average work function³⁵ and is indicated by the solid line in Fig. 6.

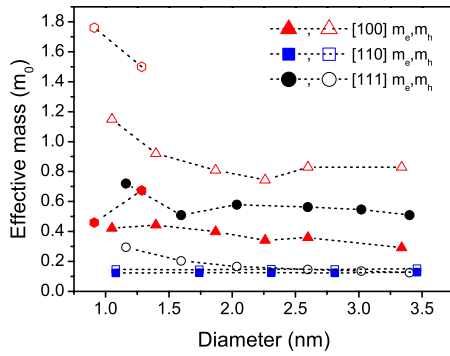


FIG. 7. (Color online) Effective mass for electrons (solid) and holes (empty) versus diameter for SiNWs. The results shown by hexagonal symbols are from two [100] wires that have a different shape than other [100] wires.

In Fig. 6, we also show the *GW* corrections to the VB and CB edges. The corrections to the VB edges are in general much smaller than those to the CB edges. For example, the VB edges for [100] wires with $d=0.91$, 1.05, and 1.29 nm decrease by 0.66, 0.72, and 0.29 eV, respectively, after including the self-energy corrections, while the CB edges are upshifted by 1.70, 1.34, and 1.57 eV, respectively.

B. Effective masses

The effective mass of the carriers in nanowires is one of the important parameters controlling their transport properties. For example, the electron thermal velocity is inversely proportional to the square root of the transport effective mass. It has been pointed out that the parabolic effective-mass approximation in the *I-V* calculation for the SNWT significantly overestimates SNWT threshold voltages when the wire width is less than 3 nm.¹⁶ Due to the two-dimensional quantum confinement, the bulk crystal symmetry is not preserved in Si nanowires, hence quantitative results obtained from the parabolic effective-mass approximation are expected to contain errors when the nanowire diameter is small. Thus, it is desirable to calculate the effective mass based on direct electronic band structure calculations for the wires.

The effective mass can be determined from the dispersion relation at the band edge using $m^* = \hbar^2 / (\partial^2 E / \partial^2 k_z)$. In Fig. 7, we show the results for both electrons and holes in the nanowires with different orientations. First, in the [110] wire, the effective mass of the carriers varies very little, $m_e \approx m_h \approx 0.18m_0$. Our calculations show that the curvature of the valence-band edge (hole effective mass) of the [110] wire is insensitive to the wire width, and resembles the result from the projected bulk band structure for this orientation. In contrast, both the effective masses of electrons and holes in the [100] and [111] wires show noticeable size dependence, although the change is not monotonically. More detailed analysis shows that the effective masses for the [111] wires also

reflect the features in the projected bulk bands, and approach to the right limits as the diameter increases. For the [100] direction, the analysis of the effective mass based on the bulk projected bands becomes much more complicated.

Our results show that the effective masses in the [100] and [111] wires, except for the hole effective mass in the [111] wires, are much larger than those of the [110] wires. We also notice that $m_e \ll m_h$ in the [100] wires, while $m_e \gg m_h$ in the [111] wires. Generally, the wires tend to exhibit a larger transport effective mass in a smaller wire, where stronger quantum confinement occurs. Vo *et al.*²¹ also studied the electron and hole masses for SiNWs in different growth directions. Similar results are obtained compared with our work: the effective masses for the [110] wires are almost independent of the wire size, while the values decrease with increasing diameter along the [001] direction.

In addition, we note that for the [100] directions, the two wires with diameters of $d=0.91$ nm and $d=1.29$ nm, respectively, have quite different effective masses (shown by hexagonal symbols) compared with other [100] SiNWs, indicating that the effective masses are strongly dependent on the cross-sectional shape.

The effective-mass values presented here are obtained from LDA energy bands, and therefore the *k*-point dependency of the *GW* corrections, if any, is expected to affect the final results.

IV. CONCLUSIONS

In conclusion, we have studied from first principles the electronic properties of SiNWs oriented in the [100], [110], and [111] directions as a function of diameter. These properties are strongly influenced by quantum confinement, showing size and orientation dependence. Direct fundamental band gaps are found at $\bar{\Gamma}$ for the [100], [110], and small [111] wires, which increase subquadratically with the inverse of diameter. It is also found that [100] and [111] wires have overall a larger gap than [110] wires, as expected from the effective-mass difference. The underestimation of band gaps by LDA is rectified by the *GW* self-energy corrections, which turns out to be surprisingly sensitive to the wire size. We have also calculated the effective masses in these SiNWs and identified in most cases the connection between the magnitude of the effective mass in the SiNWs and the features in the projected bulk bands along the specific direction.

ACKNOWLEDGMENTS

This work is supported by the National Science Foundation (Grant No. DMR-02-05328). The computation used resources of National Energy Research Scientific Computing Center (NERSC), which is supported by the U.S. Department of Energy (Grant No. DE-AC03-76SF00098), and San Diego Supercomputer Center (SDSC) at UCSD. We acknowledge the use of the PARATEC package at NERSC.

*Present address: Department of Physics, University of California at Berkeley, CA 94720, and Materials Sciences Division, Lawrence Berkeley National Laboratory, Berkeley, CA 94720.

- ¹J. D. Holmes, K. P. Johnston, R. C. Doty, and B. A. Korgel, *Science* **287**, 1472 (2000).
- ²Y. Cui and C. M. Lieber, *Science* **291**, 851 (2001).
- ³D. Katz, T. Wizansky, O. Millo, E. Rothenberg, T. Mokari, and U. Banin, *Phys. Rev. Lett.* **89**, 086801 (2002).
- ⁴D. D. Ma, C. S. Lee, F. C. K. Au, S. Y. Tong, and S. T. Lee, *Science* **299**, 1874 (2003).
- ⁵R. S. Friedman, M. C. McAlpine, D. S. Ricketts, D. Ham, and C. M. Lieber, *Nature (London)* **434**, 1085 (2005), and references therein.
- ⁶For a review, see D. J. Sirbully, M. Law, H. Yan, and P. Yang, *J. Phys. Chem. B* **109**, 15190 (2005).
- ⁷Y. Huang, X. Duan, Y. Cui, L. J. Lauhon, K. H. Kim, and C. M. Lieber, *Science* **294**, 1313 (2001).
- ⁸Y. Cui, Q. Wei, H. Park, and C. M. Lieber, *Science* **293**, 1289 (2001).
- ⁹M. H. Huang, S. Mao, H. Feick, H. Yan, Y. Wu, H. Kind, E. Weber, R. Russo, and P. Yang, *Science* **292**, 1897 (2001).
- ¹⁰X. Duan, Y. Huang, Y. Cui, J. Wang, and C. M. Lieber, *Nature (London)* **409**, 66 (2001).
- ¹¹A. M. Morales and C. M. Lieber, *Science* **279**, 208 (1998).
- ¹²Y. Cui, L. J. Lauhon, M. S. Gudiksen, J. Wang, and C. M. Lieber, *Appl. Phys. Lett.* **78**, 2214 (2001).
- ¹³L. T. Canham, *Appl. Phys. Lett.* **57**, 1046 (1990).
- ¹⁴X. Duan, J. Wang, and C. M. Lieber, *Appl. Phys. Lett.* **76**, 1116 (2000).
- ¹⁵Jing Wang, A. Rahman, A. Ghosh, G. Klimeck, and M. Lundstrom, *Appl. Phys. Lett.* **86**, 093113 (2005).
- ¹⁶Jing Wang, A. Rahman, A. Ghosh, G. Klimeck, and M. Lundstrom, *IEEE Trans. Electron Devices* **52**, 1589 (2005).
- ¹⁷A. J. Read, R. J. Needs, K. J. Nash, L. T. Canham, P. D. J. Calcott, and A. Qteish, *Phys. Rev. Lett.* **69**, 1232 (1992).
- ¹⁸F. Buda, J. Kohanoff, and M. Parrinello, *Phys. Rev. Lett.* **69**, 1272 (1992).
- ¹⁹M. S. Hybertsen and M. Needels, *Phys. Rev. B* **48**, 4608 (1993).
- ²⁰B. Delley and E. F. Steigmeier, *Appl. Phys. Lett.* **67**, 2370 (1995).
- ²¹T. Vo, A. J. Williamson, and G. Galli, *Phys. Rev. B* **74**, 045116 (2006).
- ²²R. Rurali and N. Lorente, *Phys. Rev. Lett.* **94**, 026805 (2005).
- ²³J. Li and A. J. Freeman, *Phys. Rev. B* **74**, 075333 (2006).
- ²⁴J. X. Cao, X. G. Gong, J. X. Zhong, and R. Q. Wu, *Phys. Rev. Lett.* **97**, 136105 (2006).
- ²⁵X. Zhao, C. M. Wei, L. Yang, and M. Y. Chou, *Phys. Rev. Lett.* **92**, 236805 (2004).
- ²⁶Y. Cui, Z. Zhong, D. Wang, W. U. Wang, and C. M. Lieber, *Nano Lett.* **3**, 149 (2003).
- ²⁷Y. Wu, Y. Cui, L. Huynh, C. J. Barrelet, D. C. Bell, and C. M. Lieber, *Nano Lett.* **4**, 433 (2004).
- ²⁸N. Troullier and J. L. Martins, *Phys. Rev. B* **43**, 1993 (1991).
- ²⁹M. S. Hybertsen and S. G. Louie, *Phys. Rev. B* **34**, 5390 (1986), and references therein.
- ³⁰G. Onida, L. Reining, R. W. Godby, R. Del Sole, and W. Andreoni, *Phys. Rev. Lett.* **75**, 818 (1995).
- ³¹M. Rohlfing, and S. G. Louie, *Phys. Rev. B* **62**, 4927 (2000).
- ³²C. D. Spataru, S. Ismail-Beigi, L. X. Benedict, and S. G. Louie, *Appl. Phys. A: Mater. Sci. Process.* **78**, 1129 (2004).
- ³³C. Delerue, G. Allan, and M. Lannoo, *Phys. Rev. B* **48**, 11024 (1993).
- ³⁴C.-Y. Yeh, S. B. Zhang, and A. Zunger, *Phys. Rev. B* **50**, 14405 (1994).
- ³⁵J. A. Dillon, Jr. and H. E. Farnsworth, *J. Appl. Phys.* **29**, 1195 (1958); here we take the average of work functions for three surfaces: (100), (110), and (111), and plot the average value of -4.73 eV.
- ³⁶M. Bruno, M. Palummo, A. Marini, R. Del Sole, and S. Ossicini, *Phys. Rev. Lett.* **98**, 036807 (2007).
- ³⁷C. A. Rozzi, D. Varsano, A. Marini, E. K. U. Gross, and A. Rubio, *Phys. Rev. B* **73**, 205119 (2006).